Growth Rate Determination through Automated TEM Image Analysis

Oosthoek, Jasper L. M.; Kooi, Bart J.; De Hosson, Jeff T. M.; Wolters, Rob A. M.; Gravesteijn, Dirk J.; Attenborough, Karen

Published in:
Microscopy and Microanalysis

DOI:
10.1017/S1431927610000176

Publication date:
2010

Microsc. Microanal. 16, 291–299, 2010
doi:10.1017/S1431927610000176

Microscopy AND Microanalysis

Growth Rate Determination through Automated TEM Image Analysis: Crystallization Studies of Doped SbTe Phase-Change Thin Films

Jasper L.M. Oosthoek,[1] Bart J. Kooi,[1,*] Jeff T.M. De Hosson,[1] Rob A.M. Wolters,[2] Dirk J. Gravesteijn,[2] and Karen Attenborough[3]

[1]*Materials Innovation Institute M2i and Zernike Institute for Advanced Materials, University of Groningen, Nijenborgh 4, 9747 AG, Groningen, The Netherlands*
[2]*NXP-TSMC Research Center, High Tech Campus 4, 5656 AE Eindhoven, The Netherlands*
[3]*NXP-TSMC Research Center, Kapeldreef 75, 3001 Leuven, Belgium*

Abstract: A computer-controlled procedure is outlined here that first determines the position of the amorphous-crystalline interface in an image. Subsequently, from a time series of these images, the velocity of the crystal growth front is quantified. The procedure presented here can be useful for a wide range of applications, and we apply the new approach to determine growth rates in a so-called fast-growth-type phase-change material. The growth rate (without nucleation) of this material is of interest for comparison with identical material used in phase-change random access memory cells. Crystal growth rates in the amorphous phase-change layers have been measured at various temperatures using *in situ* heating in a transmission electron microscope. Doped SbTe films (20 nm thick) were deposited on silicon nitride membranes, and samples with and without silicon oxide capping layer were studied. The activation energy for growth was found to be 3.0 eV. The samples without capping layer exhibit a nucleation rate that is an order of magnitude higher than the samples with a silicon oxide capping layer. This difference can be attributed to the partial oxidation of the phase-change layer in air. However, the growth rates of the samples with and without capping are quite comparable.

Key words: growth rate, phase-change material, doped SbTe, crystallization, amorphous-crystalline interface, TEM, *in situ* heating, image processing, blanket layer, PRAM

Introduction

A quantitative analysis of growth phenomena in a series of images is of importance for a wide range of fundamentally oriented and application-driven studies. For example, crystal growth in amorphous films is the rate-limiting step in rewritable data storage based on phase-change materials (Wuttig & Yamada, 2007). These materials have been successfully applied in rewritable optical recording based on the well-known CD, DVD (Satoh & Yamada, 2001), and Blu-ray Disc (Hellmig et al., 2003) formats. Currently, phase-change materials are extensively tested as the storage element in nonvolatile solid-state electrical memory generally called phase-change random access memory (PRAM). PRAM is one of the most promising candidates to replace Flash memory in the near future (Bez & Pirovano, 2004; Hudgens & Johnson, 2004; Cho et al., 2005; Lankhorst et al., 2005; Chen et al., 2006; Lacaita, 2006).

Flash memory is currently the technology for nonvolatile memory applications. Even though Flash memory exceeded the expectations that were foreseen in the past, it is expected that further downscaling is no longer possible (Hudgens & Johnson, 2004; Lankhorst et al., 2005). PRAM, on the other hand, is scalable using the next generations of lithography, requires less lithographic steps, has a higher (over)writing speed, and uses less program energy (Bez & Pirovano, 2004; Hudgens & Johnson, 2004; Cho et al., 2005; Lankhorst et al., 2005; Chen et al., 2006; Lacaita, 2006).

PRAM is based on a large, i.e., typically three orders of magnitude, difference in electrical resistivity between the amorphous and crystalline phase. A nanosized resistor made from phase-change material is brought to the amorphous state by a short high energy RESET pulse. During the pulse the material melts. Because the material cools rapidly after the pulse, it is quenched into the high resistance amorphous state. A longer and lower energy SET pulse, still in the submicrosecond range, heats the resistor to a temperature above the glass transition temperature but below the melting temperature. During this pulse, crystals nucleate and grow until the cell is fully crystallized to a low resistance state. The amorphous state is meta-stable, and therefore undesired spontaneous crystal growth and nucleation can occur at any temperature (below the melting temperature). However, because these processes are thermally activated,

Received September 18, 2009; accepted January 19, 2010
*Corresponding author. E-mail: B.J.Kooi@rug.nl

only the high operating temperatures (typically above 80°C) limit memory retention times (i.e., how long the amorphous state is stable at a certain temperature). The process of memory retention and cell degradation upon cycling in phase-change line cells is not yet fully understood (Lankhorst et al., 2005). In this article the crystallization of blanket films is being investigated as viable comparison with (the retention behavior of) the identical material employed in these line cells.

Generally, the process of crystallization can be separated into two different physical phenomena: nucleation and growth (Zhou, 2001; Ruitenberg et al., 2002). The phase-change material studied here is a so-called fast-growth type material. Probably more appropriate would be to call it a slow-nucleation type material. However, in many applications nucleation is not required or even undesirable, and therefore these materials can be exploited in high-speed and high-density storage applications such as Blu-ray rewritable disks (Borg et al., 2001; Khulbe et al., 2002; Oomachi et al., 2002; Her et al., 2003; Her & Hsu, 2003; Lankhorst et al., 2003), where the amorphous marks are relatively small. Also, the PRAM cells already have a crystalline area at the boundary of the amorphous mark from which crystallization can progress. Therefore, when PRAM cells are produced from a fast-growth material, the crystallization in this material can be fast and in principle only depends on growth (nucleation does not occur) (Meinders & Lankhorst, 2003; Lankhorst et al., 2005).

Although this study is based on phase-change blanket layers, the crystal growth rate (i.e., without nucleation) of this material is of interest for a comparison with (the retention behavior of) identical material and layer thickness used in PRAM cells of the line-cell geometry (Castro et al., 2007; Goux et al., 2009). A new procedure and algorithm are presented in this study that provide direct measurements of the pure crystal growth rate without having problems associated with variable growth directions, variable boundary shapes, or new nucleation events.

In the past we have extensively employed *in situ* heating in a transmission electron microscope (TEM) to determine the crystal growth rates (and to a lesser extent nucleation rates) in various types of phase-change materials (Kooi & De Hosson, 2004; Kooi et al., 2005; Pandian et al., 2006). The growth rates were obtained from a sequence of TEM images recorded at constant temperature as a function of crystallization time. To derive these growth rates, the positions of the crystallization fronts in such a sequence were determined visually. This weak point of visual judgment has been removed in our present analysis, and all analysis is automated. Therefore, the present work shows a major improvement with respect to earlier published results of the crystal growth analysis in phase-change thin films (Petfordlong et al., 1995; Morilla et al., 1996; Ruitenberg et al., 2002; Privitera et al., 2003; Kalb et al., 2004; Kooi & De Hosson, 2004; Kooi et al., 2005; Pandian et al., 2006).

Moreover, the procedures we present here are of importance for a wide range of applications where the growth rate has to be analyzed quantitatively from a series of images.

Materials and Methods

Fast-growth doped SbTe thin films with a thickness of 20 nm were deposited using DC magnetron sputtering on commercially available 25 nm thick silicon nitride TEM windows. On top of each phase-change film, a 20 or 50 nm thick silicon oxide layer was deposited by radio-frequency magnetron sputtering. Such an oxide layer is essential for protective purposes as we will show below, but also allows a closer comparison with the line cells where the phase-change line is surrounded by the identical oxide. For comparison also phase-change films without oxide capping layer have been investigated.

Samples were isothermally annealed at 160°C, 165°C, 170°C, and 175°C by *in situ* heating in a TEM (JEOL 2010F operating at 200 kV). The highest temperature is limited by the requirement that crystal nucleation should not occur during heating, but only after stabilization at the desired annealing temperature. The lowest temperature is limited by the nucleation time, which has to be sufficiently small (within hours) for a practical measurement.

TEM images were taken at regular intervals after nucleation had taken place. For each temperature a complete series typically consisting of 30 images was taken. Figure 1 shows a selection of images from one series.

The temperature of the TEM sample holder was accurately controlled with a Gatan model 901 SmartSet Hot Stage Controller. It employs a PID controller that allows accurate control of the temperature within ± 0.5°C. A desired final temperature can be reached with a fast ramp rate without overshoot.

The temperature of the area that is imaged within the TEM is generally lower than the temperature of the furnace in the holder. This is because the sample consists of a very thin sheet surrounded by a vacuum. All the thermal energy has to be conducted through the sheet itself. Therefore, all measurements were performed on an area nearest to the edge of the silicon nitride window (i.e., as close as possible to the thick Si wafer). This can be seen in Figure 1 where the silicon substrate shows up as dark corners (bottom left and right). Moreover, the edge of the window could be used to correct for image drift during heating caused by thermal expansion of the TEM sample holder.

Results and Discussion

Typical examples of TEM images recorded during the *in situ* heating at 165°C are shown in Figure 1. Crystals can be observed readily because they are imaged both clearly

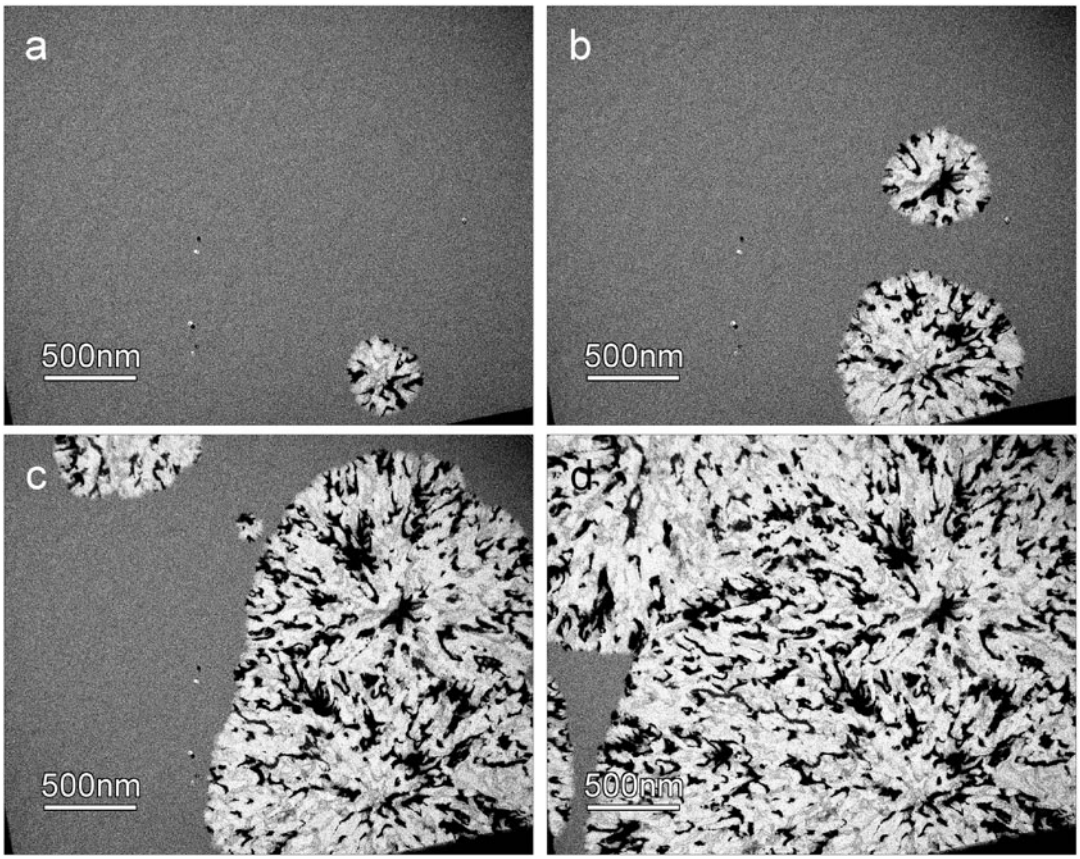

Figure 1. Plane view bright-field TEM images of a 20 nm thick, initially amorphous doped SbTe phase-change film (between 25 nm silicon nitride and 50 nm silicon oxide layers) taken 6, 14, 24 and 37 min after reaching 165°C.

brighter and darker than the surrounding amorphous phase. This black and white contrast of the crystals is peculiar and is caused by the transrotational nature of the crystal structure (Kolosov & Tholen, 2000; Kooi & De Hosson, 2004). Previous crystallization studies on similar fast growth materials were performed without a capping layer (Kooi et al., 2004; Kooi & De Hosson, 2004). During crystallization the phase-change material shrinks slightly because of the difference in density between the amorphous and the crystalline phase. The amorphous layers of the samples have a free surface where bending can occur (Kooi & De Hosson, 2004). The combined action of densification with movement of the crystallization front results in bending of the crystal lattice planes. These crystals tend to have a regular (often threefold symmetrical) bending shape. The amorphous phase-change layer in the present study is sandwiched between a silicon oxide and silicon nitride layer. A free surface is therefore absent. Bending in this situation is constrained and explains the more random black and white contrast associated with the transrotational crystal structure. From the sequence of images in Figure 1, it is clear that crystals nucleate at random locations and grow with a more or less circular shape.

The importance of the silicon oxide capping layer is shown in Figure 2, where Figures 2a and 2b show phase-change films, partially crystallized at 160°C, with and without capping layer, respectively. The annealing experiment/crystallization took place about two weeks after deposition and keeping the samples in air. The crystallization of the phase-change film without capping proceeds much faster because of the shorter incubation times for nucleation and because of a much higher nucleation rate and thus nucleation density (because the growth rate is not strongly influenced, see also the Growth Rate as a Function of Temperature section below). Partial (surface) oxidation of the phase-change film can be held responsible for the increased nucleation rate and the reduction in crystallization temperature. Similar results were observed for $Ge_2Sb_2Te_5$ films (Kooi et al., 2004).

Although TEM images represent two-dimensional (2D) projections of a three-dimensional structure, the present analysis can be purely 2D because the crystallites to be analyzed have sizes that are much larger than the 20 nm thickness of the phase-change film. To determine the crystal growth rate(s) at a certain temperature, it is first required to quantify the position of the interface between the amor-

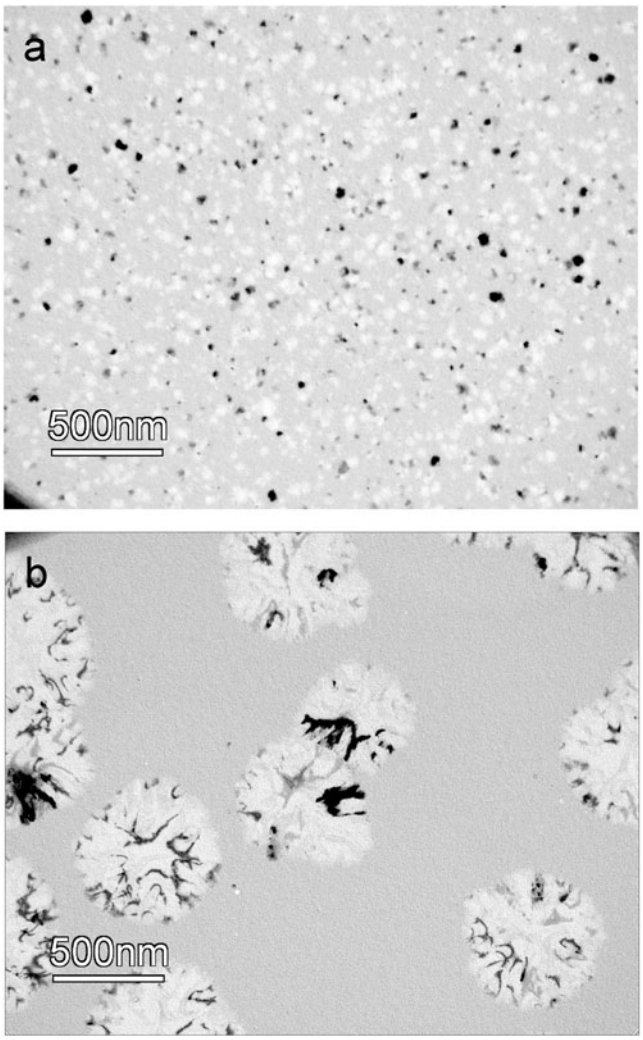

Figure 2. Plane view bright-field TEM images of 20 nm thick doped SbTe phase-change films partially crystallized at 160°C. **a:** Phase-change film capped with 50 nm thick silicon oxide. **b:** Phase-change film without capping layer. Note the much higher nucleation density in case the capping layer is absent.

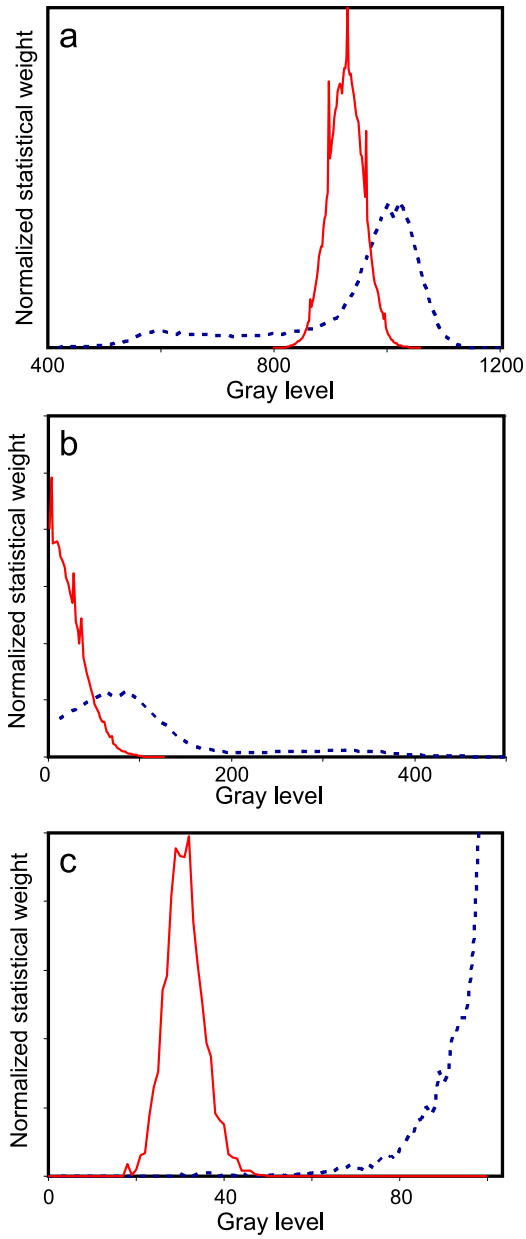

Figure 3. (color online) Each figure shows a histogram of the amorphous phase (solid line) and crystalline phase (dashed line). **a:** Original image. The two histograms overlap. **b:** After filter step 1 (see article text for details). The two histograms still overlap considerably. The crystalline phase has a few isolated bright spots that are removed in step 2 (not shown). **c:** After filter step 3, the MLV filter has led to a complete separation of the two histograms.

phous and crystalline phase. The procedure to do this is explained in the next section.

Image Filtering: Detecting the Amorphous-Crystalline Interface

Figure 1 illustrates that geometrical information can only be used at an early stage of crystallization. Crystals nucleate at random locations and merge with one another to form odd crystal shapes with no well-defined centers or radii and where after merging the crystal boundaries cannot be detected anymore. Still, the movement of the crystal boundary with time is a direct measurement of the growth rate. To quantify this movement, the location of the amorphous-crystalline interface has to be obtained from the image.

Figure 3a shows the histograms (number of pixels with a certain gray level versus the gray level) pertaining to the amorphous and crystalline phases present in an image. The amorphous phase is represented by a bell-shaped peak (solid line), whereas the crystalline phase corresponds to a histogram that extends its pixel levels over a much larger range including the one for the amorphous phase (dashed

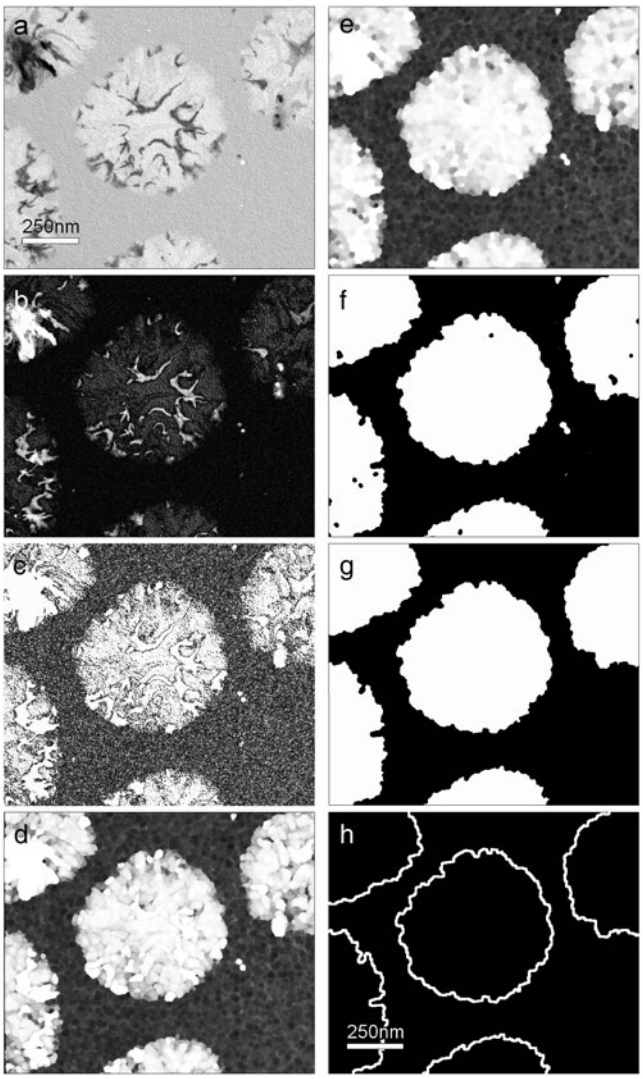

Figure 4. Series of images that show the evolution of the filter process. **a:** Subsection of an original image before filtering. **b–h:** Images after the filter steps 1 to 7 (explained in detail in the article text), respectively.

line). Therefore, regions in the crystalline area exist with the same pixel level as found in the amorphous phase. Also the image has a considerable amount of noise. A simple threshold operation to separate the two phases apparently does not work. As a solution, a seven-step filter procedure was designed that yields excellent results in producing the exact position of the crystal-growth front. The seven steps are summarized as follows:

1. The crystalline phase consists of areas being both brighter and darker than the amorphous phase; see Figure 4a showing a part of an original (as-recorded) image. Therefore, the bright and dark gray level values have to be unified: in this step all amorphous regions become dark and all crystalline regions become bright. This is done by taking for each pixel the absolute value with respect to the average amorphous pixel value. The average pixel value of the amorphous area is obtained from the original image. This is simply done by selecting an area that is known to be amorphous and determining the gray value associated with the peak maximum in the histogram of the amorphous phase (from Fig. 3a a value of 925 was obtained). When the settings of the TEM are not changed during a single measurement, this value stays constant for all images in the series and does not have to be obtained for each image separately. The bright and dark gray levels are turned into a bright "color." The gray levels of the amorphous phase are turned into a dark "color." The resulting image is shown in Figure 4b, and the resulting histograms for the amorphous and crystalline phases after this "contrast-flip" operation are shown in Figure 3b again as a solid line and a dashed line, respectively. Although this "contrast-flip" operation largely normalizes the original bright and dark areas of the crystalline phase into bright areas, it will also create dark(er) "ribbons" at the transition between these black and a white areas in the original image. An important step is thus to remove these ribbons later (see step 4).
2. There is still unnecessary contrast in the crystalline phase after step 1. Very bright spots can be seen in Figure 4b where a dark (almost black) spot was in the original image. The crystalline phase is made more uniform by setting a maximum pixel value. A value is chosen that is just above the highest value of the amorphous phase (in this case a value of 100). Pixels that exceed 100 will be set to 100. The resulting image is shown in Figure 4c. Although the crystalline phase is more or less uniform considerable, noise is still present.
3. Applying a threshold operation after step 2 will result in a very poor quality image, and therefore image noise has to be reduced. This is done with the so-called *Mean of Least Variance* filter (MLV filter), which was published by Schulze and Pearce (1993). The MLV filter enhances the image quality by smoothing homogeneous regions without blurring the edges (see Fig. 4d). After application of the MLV filter, the histogram shows that the crystalline phase and amorphous phase now have their own well separated peak (see Fig. 3c). The structuring element used in the MLV filter (Schulze & Pearce, 1993) was circular with a typical diameter of 8 pixels.
4. Still dark regions (the ribbons, see step 1) exist in the crystalline phase where in the original image a dark area and a bright area met. These regions are further reduced by a morphological *close* operation (subsequent *dilation* and *erode* operation). The same structuring element that was used for the MLV operation was also used for the close operation. In the resulting image (Fig. 4e), a large contrast exists between the amorphous and crystalline phases.
5. After step 4 a standard *threshold* operation outputs a 1 for each pixel value above a certain chosen threshold and a 0 for each value equal or below.

6. The resulting binary (black and white) image (Fig. 4f) still has a few isolated spots. These spots are caused by noise, imperfections in the sample, or spots associated with the charge-coupled device camera. At this stage an operation *removes spots* that are smaller than a certain amount of pixels. The resulting image is shown in Figure 4g.
7. A final operation creates a growth-front image. Such an image has a line where the black and white areas in the previous image meet. See the image shown in Figure 4h, where the line is made thicker for clarity.

Image Processing: Quantifying the Growth Speed

A complete time series of TEM images is converted into binary growth-front images with the procedure delineated in the previous section. Each growth-front image is multiplied with the value of the time (in seconds) that the image was taken. Only the growth front (line) has this time value, and the rest of the image is equal to zero. Then, all these images in the series are summed to create a single final image that contains all essential information for determination of the crystal growth rate. In this single "growth-front–time" image, each growth front is represented as a line with a pixel value equal to the time (in seconds) that the image was taken. This is shown schematically in Figure 5a–c, where for reasons of visibility only a small selection of the total number of TEM images was taken to create larger steps in time (see Fig. 5c). The brighter the line the later in time the original image was taken.

At each position in the time image, a statistically averaged value of the slope is found by fitting a surface to that position and all points around it with a distance less than or equal to r pixels (see Fig. 5d). Only the pixels that are on a growth front are used for the fit; the black pixels (value of zero) are omitted. This last point is important for obtaining accurate results. The radius r is chosen such that the circle contains several growth boundaries. The spatial components a and b of the fitted surface ($ax + by + t = c$) have the units time per pixel and represent the inverse growth rate and direction. The average growth rate G (nm/s) is obtained from the spatial components a and b and has the value $G = \Delta D / \sqrt{a^2 + b^2}$, where ΔD is the physical size in nm of a pixel. The final result presenting the growth rate is shown in Figure 5d.

Our procedure is very useful to determine the evolution of growth rate with time or crystal size (or growth-front curvature). However, our analysis shows that the crystal growth rate in our present phase-change system does not depend on time, and therefore the gray level in Figure 5e is relatively uniform (except for the boundaries where the growing crystals coalesce because a singularity occurs in the computer-controlled determination of the growth rate).

Many traditional methods for quantifying the kinetics of phase transformations rely on the determination of the total transformed volume or area fraction as a function of time. If the area fraction is based on an image where the boundary between the two phases has to be assessed, the detected boundary can be found at an offset from the location of the actual boundary. This offset will depend on the applied filter method and sensitivity. The higher the ratio between boundary length and surface area (the smaller the crystals), the larger the error due to an offset will be. The total transformed area will therefore depend on the size of the crystallite and the filter method and its evolution and

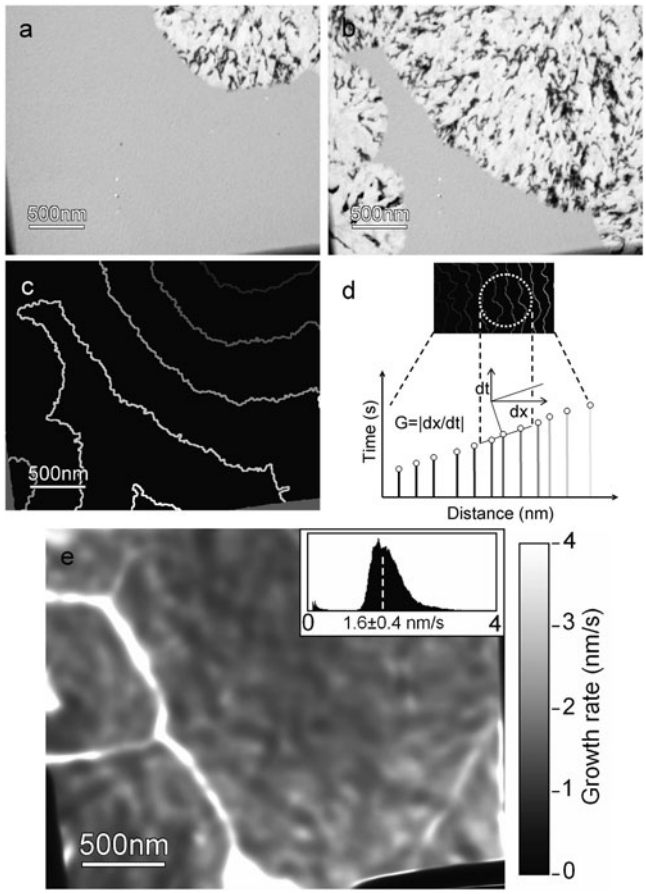

Figure 5. Determination of growth rate from a series of TEM images. A sample was annealed at 170°C and an image was taken every 30 s. **a:** TEM image taken 8.5 min after reaching 170°C. **b:** TEM image taken exactly 10 min after Figure 5a. **c:** Figure showing the growth fronts of the series for 5 min intervals (where each minute a TEM image was recorded). The lines are made thicker for visibility. **d:** Schematic representation of the determination of the growth rate from the growth fronts. At each position a surface is fit to the gray (nonzero) points that are on a growth front and are located within a circle centered at that position. From the spatial components (**a** and **b**) of the surface ($ax + by + t = c$), the growth rate is calculated: G (nm/s) = ΔD (nm/pixel)/$\sqrt{(a^2 + b^2)}$. **e:** From the complete set of TEM images, the growth rate is calculated for each position. The inset shows a histogram of the value of the growth rate. A growth rate of 1.6 ± 0.4 nm/s was obtained (based on full-width at half-maximum).

is thus susceptible for having a relatively large systematic error.

The method proposed here is only sensitive to the movement of the boundary. A fixed offset that is shared by two boundaries will not show up in the time image because it is based on the slope (derivative). Also, the method proposed here allows for a spatial and time dependent measurement of the growth rate. Even a nonlinear growth rate (time dependent growth rate) in principle can be quantified. This makes the procedures delineated in the present article of importance for a wide range of applications analyzing an evolution rate in a series of images. Particularly applications where one entity is growing at the expense of another entity and where the gray levels in the image of the two entities are (partially) overlapping.

Growth Rate as a Function of Temperature

Samples with an oxide capping layer were annealed *in situ* in the TEM at 160°C, 165°C, 170°C, and 175°C. For each data point a new sample was used. The closed square data points represent samples with a 50 nm silicon oxide capping layer, and for the closed triangular data points the capping layer was 20 nm. After nucleation had occurred a series of images was recorded at constant time intervals until the area was crystallized. It was found that only the area that had been irradiated by the electron beam was completely crystallized. Crystals did appear in the area outside the irradiated area, but these were smaller. These results indicate that the electron beam of the TEM increases the nucleation rate (decreases incubation time for nucleation) and may also increase the growth rate. The average growth rate of the oxide capped samples, as obtained from the images with the procedures described in the previous two sections, is shown versus the reciprocal temperature in Figure 6 (closed squares). No difference in growth was found between the samples capped with 20 and 50 nm silicon oxide. Assuming an Arrhenius-type dependence of the growth rate on temperature, an activation energy of 3.0 ± 0.1 eV is determined from fitting the data.

Samples without capping layer were also annealed *in situ* in the TEM at 155°C and 160°C. The growth rates measured for these samples at these temperatures are shown in Figure 6 as open circles. These samples had been kept in air for two weeks prior to the measurements. The amount of nuclei per unit area counted after complete crystallization of the imaged area was at least an order of magnitude larger than the amount found in the previous cases with oxide capping layer (cf. Fig. 2). Apparently exposing the phase-change film to air greatly increases the nucleation rate. This can be attributed to partial oxidation of the phase-change layer, which apparently forms starting points for nucleation and thus lowers the activation energy barrier required for nucleation.

Because of the large amount of nuclei present in the samples without oxide capping layer, the distance a crystalline mark can grow before it meets another mark is much smaller. This also makes the measurement of the growth rate more susceptible to drift of the image. These variations of the location of the crystalline mark will not influence the average of the growth rate because the crystals grow outward in all directions. Still, the error bar of the growth rate of these samples is definitely larger (open circles). However, the present results still clearly show that despite the large differences in the nucleation rate, the growth rate of the samples with and without oxide capping layer are nearly the same.

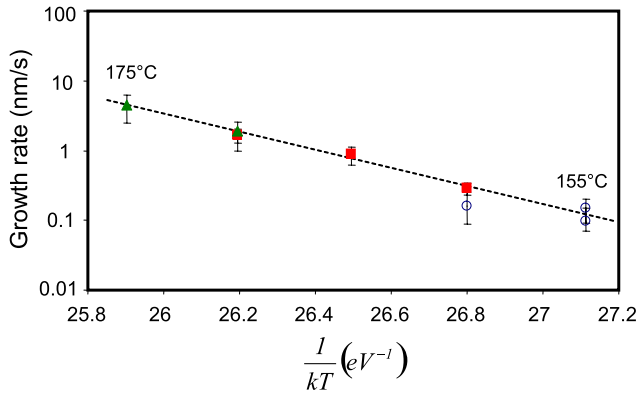

Figure 6. (color online) Arrhenius plot showing the growth rate of the samples with silicon oxide capping layer (triangles, 20 nm; squares, 50 nm) and without (circles) capping layer. The dashed line is a fit to the triangular and square data points only. Extrapolation to 155°C shows that growth rate of the samples without capping layer is the same as the growth rate of the samples with capping layer.

To confirm the influence of the electron beam on the growth rate, a measurement at a (2.5×) higher magnification was performed, i.e., irradiation occurs with a (6.25×) higher current density. This measurement was performed on a sample without oxide capping layer at 155°C on an area that was not previously exposed to the electron beam, but the sample itself was already annealed for 30 min at 155°C. The region that was not irradiated was still largely amorphous with only a few nuclei. In this second measurement, nucleation had thus taken place without the presence of the electron beam. The average growth rate is slightly (but, in principle, not significantly) larger than average growth rate of the previous measurement that had been nucleated in the presence of the electron beam. This result seems to indicate that the growth rate is not strongly increased by electron irradiation and that the previously mentioned difference between overall crystallization rate can largely be attributed to an increased nucleation rate in the electron beam exposed area. However, we also observed that the growth rate in previously thermally annealed areas is slightly but significantly lower than in areas during thermal annealing that are from the beginning also continuously irradiated by the electron beam. Therefore, both effects—an increased growth rate due to an increased elec-

tron beam current density and a decreased growth rate due to a previous thermal anneal (without electron beam exposure)—appear to have compensated each other.

Conclusions

An image filter procedure (algorithm) has been presented in this study that allows discrimination (threshold) between two entities (e.g., phases) where the gray levels in the image of one entity are overlapping with those of the other entity. Subsequently, an image processing procedure has been presented that allows the determination of the evolution rate in a series of images, where one entity is growing at the expense of another entity. This procedure directly quantifies the pure growth rate without being affected by factors such as varying growth directions, varying boundary shapes during growth, or new nucleation events. The procedures were particularly developed to analyze the crystal growth rate in initially amorphous phase-change thin films. The growth rates were obtained from a sequence of TEM images recorded at constant temperature as a function of crystallization time. The present work presents a major improvement with respect to results published earlier on crystal growth rates in phase-change films, where the position of the growth front was based on visual judgment.

To exemplify details of the procedure, blanket doped SbTe films (20 nm thick) deposited on silicon nitride membranes and capped with 20 or 50 nm silicon oxide were isothermally heated inside a TEM. The activation energy for pure growth was found to be 3.0 eV (assuming an Arrhenius-type dependence of growth rate on temperature). The results show that samples without any capping layer had an order of magnitude higher nucleation rate than samples with silicon oxide capping layer. This difference can be attributed to the partial oxidation of the phase-change layer in air. However, interestingly the growth rates of the samples with and without capping layers were comparable.

Acknowledgments

The research was carried out under project number MC3.05241 in the framework of the Strategic Research Programme of the Materials Innovation Institute M2i (the former Netherlands Institute for Metals Research or NIMR). Financial support from the M2i is gratefully acknowledged.

References

Bez, R. & Pirovano, A. (2004). Non-volatile memory technologies: Emerging concepts and new materials. *Mater Sci Semicond Process* **7**, 349–355.

Borg, H.J., Van Schijndel, M., Rijpers, J.C.N., Lankhorst, M.H.R., Zhou, G.F., Dekker, M.J., Ubbens, I.P.D. & Kuijper, M. (2001). Phase-change media for high-numerical-aperture and blue-wavelength recording. *Jpn J Appl Phys* **40**, 1592–1597.

Castro, D.T., Goux, L., Hurkx, G.A.M., Attenborough, K., Delhougne, R., Lisoni, J., Jedema, F.J., Zandt, M.A.A., Wolters, R.A.M., Gravesteijn, D.J., Verheijen, M., Kaiser, M., Weemaes, R.G.R. & Wouters, D.J. (2007). Evidence of the thermo-electric Thomson effect and influence on the program conditions and cell optimization in phase-change memory cells. In *IEEE International Electron Devices Meeting*, pp. 315–318. Washington, DC: IEEE.

Chen, Y.C., Rettner, C.T., Raoux, S., Burr, G.W., Chen, S.H., Shelby, R.M., Salinga, M., Risk, W.P., Happ, T.D., McCleland, G.M., Breitwisch, M., Schrott, A., Philipp, J.B., Lee, M.H., Cheek, R., Nirschl, T., Lamorey, M., Chen, C.F., Joseph, E., Zaidi, S., Yee, B., Lung, H.L., Bergmann, R. & Lam, C. (2006). Ultra-thin phase-change bridge memory device using GeSb. In *IEEE International Electron Devices Meeting*, pp. 1–4. San Francisco, CA: IEEE.

Cho, W.Y., Cho, B.-H., Choi, B.-G., Oh, H.-R., Kang, S., Kim, K.-S., Kim, K.-H., Kim, D.-E., Kwak, C.-K., Byun, H.-G., Hwang, Y., Ahn, S., Koh, G.-H., Jeong, G., Jeong, H. & Kim, K. (2005). A 0.18-μm 3.0-V 64-Mb nonvolatile phase-transition random access memory (PRAM). *IEEE J Solid-State Circ* **40**, 293–300.

Goux, L., Castro, D.T., Hurkx, G.A.M., Lisoni, J.G., Delhougne, R., Gravesteijn, D.J., Attenborough, K. & Wouters, D.J. (2009). Degradation of the reset switching during endurance testing of a phase-change line cell. *IEEE Trans Electron Devices* **56**, 354–358.

Hellmig, J., Mijiritskii, A.V., Borg, H.J., Musialkova, K. & Vromans, P. (2003). Dual-layer Blu-ray Disc based on fast-growth phase-change materials. *Jpn J Appl Phys* **42**, 848–851.

Her, Y.C., Chen, H. & Hsu, Y.S. (2003). Effects of Ag and In addition on the optical properties and crystallization kinetics of eutectic $Sb_{70}Te_{30}$ phase-change recording film. *J Appl Phys* **93**, 10097–10103.

Her, Y.C. & Hsu, Y.S. (2003). Optical properties and crystallization characteristics of Ge-doped $Sb_{70}Te_{30}$ phase change recording film. *Jpn J Appl Phys* **42**, 804–808.

Hudgens, S. & Johnson, B. (2004). Overview of phase-change chalcogenide nonvolatile memory technology. *MRS Bull* **29**, 829–832.

Kalb, J., Spaepen, F. & Wuttig, M. (2004). Atomic force microscopy measurements of crystal nucleation and growth rates in thin films of amorphous Te alloys. *Appl Phys Lett* **84**, 5240–5242.

Khulbe, P.K., Hurst, T., Horie, M. & Mansuripur, M. (2002). Crystallization behavior of Ge-doped eutectic Sb70Te30 films in optical disks. *Appl Opt* **41**, 6220–6229.

Kolosov, V.Y. & Tholen, A.R. (2000). Transmission electron microscopy studies of the specific structure of crystals formed by phase transition in iron oxide amorphous films. *Acta Mater* **48**, 1829–1840.

Kooi, B.J. & De Hosson, J.T.M. (2004). On the crystallization of thin films composed of $Sb_{3.6}Te$ with Ge for rewritable data storage. *J Appl Phys* **95**, 4714–4721.

Kooi, B.J., Groot, W.M.G. & De Hosson, J.T.M. (2004). *In situ* transmission electron microscopy study of the crystallization of Ge2Sb2Te5. *J Appl Phys* **95**, 924–932.

Kooi, B.J., Pandian, R., De Hosson, J.T.M. & Pauza, A. (2005). *In situ* transmission electron microscopy study of the crystallization of fast-growth doped Sb_xTe alloy films. *J Mater Res* **20**, 1825–1835.

Lacaita, A.L. (2006). Phase change memories: State-of-the-art, challenges and perspectives. *Solid State Electr* **50**, 24–31.

Lankhorst, M.H.R., Ketelaars, B. & Wolters, R.A.M. (2005). Low-cost and nanoscale non-volatile memory concept for future silicon chips. *Nat Mater* **4**, 347–352.

Lankhorst, M.H.R., Van Pieterson, L., Van Schijndel, M., Jacobs, B.A.J. & Rijpers, J.C.N. (2003). Prospects of doped Sb-Te phase-change materials for high-speed recording. *Jpn J Appl Phys* **42**, 863–868.

Meinders, E.R. & Lankhorst, M.H.R. (2003). Determination of the crystallisation kinetics of fast-growth phase-change materials for mark-formation prediction. *Jpn J Appl Phys* **42**, 809–812.

Morilla, M.C., Afonso, C.N., Petfordlong, A.K. & Doole, R.C. (1996). Influence of the relaxation state on the crystallization kinetics of Sb-rich SbGe amorphous films. *Philos Mag A* **73**, 1237–1247.

Oomachi, N., Ashida, S., Nakamura, N., Yusu, K. & Ichihara, K. (2002). Recording characteristics of Ge doped eutectic SbTe phase change discs with various compositions and its potential for high density recording. *Jpn J Appl Phys* **41**, 1695–1697.

Pandian, R., Kooi, B.J., De Hosson, J.T.M. & Pauza, A. (2006). Influence of capping layers on the crystallization of doped Sb_xTe fast-growth phase-change films. *J Appl Phys* **100**, 123511.

Petfordlong, A.K., Doole, R.C., Afonso, C.N. & Solis, J. (1995). *In-situ* studies of the crystallization kinetics in Sb-Ge films. *J Appl Phys* **77**, 607–613.

Privitera, S., Bongiorno, C., Rimini, E., Zonca, R., Pirovano, A. & Bez, R. (2003). Amorphous-to-Polycrystal Transition in GeSbTe thin films. In *Advanced Data Storage Materials and Characterization Techniques*, HH1.4. San Francisco, CA: Materials Research Society.

Ruitenberg, G., Petford-Long, A.K. & Doole, R.C. (2002). Determination of the isothermal nucleation and growth parameters for the crystallization of thin Ge2Sb2Te5 films. *J Appl Phys* **92**, 3116–3123.

Satoh, I. & Yamada, N. (2001). DVD-RAM for all audio/video, PC, and network applications. *Proc SPIE* **4085**, 283–290.

Schulze, M.A. & Pearce, J.A. (1993). Value-and-criterion filters: A new filter structure based upon morphological opening and closing. *Proc SPIE* **1902**, 106–115.

Wuttig, M. & Yamada, N. (2007). Phase-change materials for rewriteable data storage. *Nat Mater* **6**, 824–832.

Zhou, G.F. (2001). Materials aspects in phase change optical recording. *Mater Sci Eng A* **304–306**, 73–80.